PRIFYSGOL ABERYSTWYTH UNIVERSITY

Aberystwyth University

High-Pressure Transformation of SiO2 Glass from a Tetrahedral to an Octahedral Network

Zeidler, Anita; Wezka, Kamil; Rowlands, Ruth F.; Whittaker, Dean A.J.; Salmon, Philip S.; Polidori, Annalisa; Drewitt, James W.E.; Klotz, Stefan; Fischer, Henry E.; Wilding, Martin C.; Bull, Craig L.; Tucker, Matthew G.; Wilson, Mark

Published in:
Physical Review Letters

DOI:
10.1103/PhysRevLett.113.135501

Publication date:
2014

Citation for published version (APA):
Zeidler, A., Wezka, K., Rowlands, R. F., Whittaker, D. A. J., Salmon, P. S., Polidori, A., Drewitt, J. W. E., Klotz, S., Fischer, H. E., Wilding, M. C., Bull, C. L., Tucker, M. G., & Wilson, M. (2014). High-Pressure Transformation of SiO2 Glass from a Tetrahedral to an Octahedral Network: A Joint Approach Using Neutron Diffraction and Molecular Dynamics. *Physical Review Letters*, *113*(13), [135501]. https://doi.org/10.1103/PhysRevLett.113.135501

General rights
Copyright and moral rights for the publications made accessible in the Aberystwyth Research Portal (the Institutional Repository) are retained by the authors and/or other copyright owners and it is a condition of accessing publications that users recognise and abide by the legal requirements associated with these rights.

• Users may download and print one copy of any publication from the Aberystwyth Research Portal for the purpose of private study or research.
• You may not further distribute the material or use it for any profit-making activity or commercial gain
• You may freely distribute the URL identifying the publication in the Aberystwyth Research Portal

Take down policy
If you believe that this document breaches copyright please contact us providing details, and we will remove access to the work immediately and investigate your claim.

tel: +44 1970 62 2400
email: is@aber.ac.uk

Download date: 23. Sep. 2023

High-Pressure Transformation of SiO_2 Glass from a Tetrahedral to an Octahedral Network: A Joint Approach Using Neutron Diffraction and Molecular Dynamics

Anita Zeidler,[1] Kamil Wezka,[1] Ruth F. Rowlands,[1] Dean A. J. Whittaker,[1] Philip S. Salmon,[1,*] Annalisa Polidori,[1] James W. E. Drewitt,[2] Stefan Klotz,[3] Henry E. Fischer,[4] Martin C. Wilding,[5] Craig L. Bull,[6] Matthew G. Tucker,[6] and Mark Wilson[7,†]

[1]*Department of Physics, University of Bath, Bath BA2 7AY, United Kingdom*
[2]*Centre for Science at Extreme Conditions, School of Physics and Astronomy, University of Edinburgh, Edinburgh EH9 3JZ, United Kingdom*
[3]*IMPMC, CNRS UMR 7590, Université Pierre et Marie Curie, 75252 Paris, France*
[4]*Institut Laue Langevin, 6 rue Jules Horowitz, BP 156, 38042 Grenoble, France*
[5]*IMPS, Aberystwyth University, Aberystwyth SY23 3BZ, United Kingdom*
[6]*ISIS Facility, Rutherford Appleton Laboratory, Chilton, Didcot, Oxon OX11 0QX, United Kingdom*
[7]*Physical and Theoretical Chemistry Laboratory, University of Oxford, South Parks Road, Oxford OX1 3QZ, United Kingdom*

(Received 8 November 2013; revised manuscript received 7 July 2014; published 23 September 2014)

A combination of *in situ* high-pressure neutron diffraction at pressures up to 17.5(5) GPa and molecular dynamics simulations employing a many-body interatomic potential model is used to investigate the structure of cold-compressed silica glass. The simulations give a good account of the neutron diffraction results and of existing x-ray diffraction results at pressures up to ~60 GPa. On the basis of the molecular dynamics results, an atomistic model for densification is proposed in which rings are "zipped" by a pairing of five- and/or sixfold coordinated Si sites. The model gives an accurate description for the dependence of the mean primitive ring size $\langle n \rangle$ on the mean Si-O coordination number, thereby linking a parameter that is sensitive to ordering on multiple length scales to a readily measurable parameter that describes the local coordination environment.

DOI: 10.1103/PhysRevLett.113.135501 PACS numbers: 61.43.Fs, 61.05.F-, 62.50.-p, 64.70.kj

Silica is the fundamental network glass-forming material whose behavior under pressure is of long-standing interest, partly because it acts as a reference for geophysically relevant silicates [1–12]. For the glass, the primary densification mechanisms identified by experiment are associated with a reduction of the Si-O-Si bond angle between SiO_4 tetrahedra at pressures $p \lesssim 10$ GPa and with an increase in the mean Si-O coordination number $\bar{n}_{\mathrm{Si}}^{\mathrm{O}}$ from four to six at higher pressures [3–5,7–11]. These simple metrics are, however, insufficient to establish the precise atomistic mechanisms of network collapse, which may evolve over multiple length scales and be dependent on the pathway used to form the high-pressure glass [13–19]. Such information is a prerequisite for understanding the density-driven changes in material properties.

Ring statistics offer insight into glass structure over multiple length scales, where this scale depends on the total number of atoms in a ring, and provide a natural language for the density-driven structural evolution of silica glass [20]. There is a need, however, for accurate experimental information to validate the particular approach taken. For example, models in which SiO_4 tetrahedra are preserved predict a rise in the mean ring size with pressure as observed for crystalline structures [20–22], whereas models with more adaptable nearest-neighbor coordination environments suggest a more complex evolution [16–18] in which fivefold coordinated Si sites can promote the formation of smaller rings [23]. X-ray diffraction (XRD) is a key structural probe of densified silica [5–7,10,11] but it is not possible to solve the structure using this technique alone [24]. Information from other structural probes is therefore necessary in order to constrain models of silica glass under pressure, thereby helping to differentiate between the various models that can be constructed on the basis of XRD results alone.

In this Letter, we employ *in situ* high-pressure neutron diffraction (ND) to measure the structure of cold-compressed silica glass at pressures up to 17.5(5) GPa, the maximum pressure that can be reliably achieved by using the ND method [25], using an experimental approach that overcomes the major difficulties found in previous work [26]. ND is sensitive to the oxygen atom correlations and therefore provides complementary information to XRD: the weighting factors for the Si-Si, Si-O and O-O correlations in the total structure factors measured in a diffraction experiment are 0.0694:0.3880:0.5427 for ND versus 0.2178:0.4978:0.2844 for XRD at a scattering vector $k = 0$. Molecular dynamics (MD) simulations using the Tangney-Scandolo [27] (TS) interatomic potentials, which incorporate anion (dipole) polarization terms [28], are found to give a good account of *both* the ND (present work) and XRD results [6,10,11,29], as well as the

 © 2014 American Physical Society

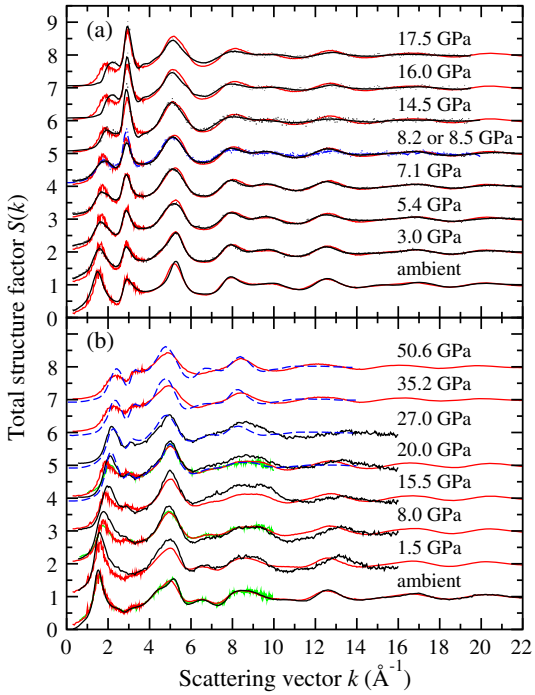

FIG. 1 (color online). The pressure dependence of the (a) neutron and (b) x-ray $S(k)$ functions. In (a), the broken (blue) curve ($p = 8.5$ GPa) and solid (black) curves (all other pressures) give spline fits to the measured data represented by the points with vertical error bars. For the experiments in the pressure range 8.5–17.5 GPa, the region $k \leq 1.55$ Å^{-1} was not accessible and the curves in this region are fitted Lorentzian functions [25]. In (b), the XRD results are from Refs. [6] [solid light (green) curves at ambient, 8.0 and 20.0 GPa], [29] [solid (black) curve at ambient], [10] [solid (black) curves at high p] and [11] [broken (blue) curves]. In (a) and (b), the solid light (red) curves show the TS MD results for the same or comparable pressures.

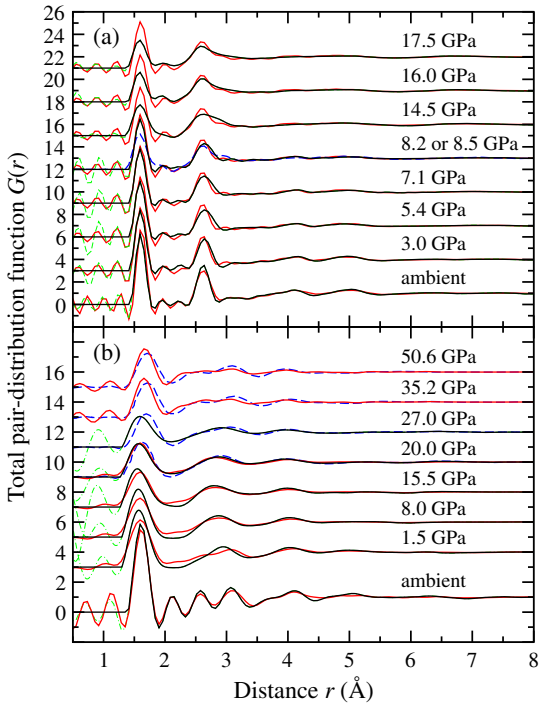

FIG. 2 (color online). The pressure dependence of the (a) neutron and (b) x-ray $G(r)$ functions. In (a), the broken (blue) curve ($p = 8.5$ GPa) and solid (black) curves (all other pressures) are the Fourier transforms of the spline fitted measured $S(k)$ functions shown in Fig. 1(a), and the broken light (green) curves show the unphysical small-r oscillations. In (b), the solid (black) curves are the Fourier transforms of the measured $S(k)$ functions shown in Fig. 1(b) from Refs. [10,29] with a cutoff $k_{\max} = 15$ Å^{-1} (and also with a Lorch [47] modification function for the Ref. [10] data), and the chained (green) curves show the unphysical small-r oscillations. The broken (blue) curves are the measured $G(r)$ functions from Ref. [11]. In (a) and (b), the solid light (red) curves are the Fourier transforms of the TS MD results given in Fig. 1, where the same modification functions were used as in experiment.

measured equation of state (see Supplemental Material [30], Fig. S1), at pressures up to ~60 GPa. A ring closure model is developed in which rings are "zipped" by a pairing of fivefold and/or sixfold coordinated Si sites. The model is in agreement with the MD results, thereby relating the pressure dependence of a parameter that is sensitive to ordering on multiple length scales to the local coordination environment in the glass.

Figures 1 and 2 compare the measured total structure factors $S(k)$ and pair-distribution functions $G(r)$ from ND (present work) and XRD with the cold-compression MD results. The XRD experiments used no pressure apparatus [29], a cubic-type multianvil press [6], or a diamond anvil cell [10,11]. Details of the ND [25,44,45] and MD work are given in the Supplemental Material [30], Sec. S2. The simulations reproduce all of the main features in the measured ND and XRD patterns at pressures up to 60 GPa, although there is a shift in position of the first sharp diffraction peak at ~2.2 Å^{-1} in the $p \sim 15$–20 GPa range, and the highest pressure ND $G(r)$ functions are damped relative to simulation (Supplemental Material [30], Sec. S3). Many of the discrepancies are comparable to those found between the different experiments, and originate from the challenges associated with experiments under extreme conditions, e.g., from the difficulty in correcting for diamond Compton scattering [46] and radiation induced annealing [11].

Figures 3(a)–3(b) show the pressure dependence of $\bar{n}_{\mathrm{Si}}^{\mathrm{O}}$ and the mean Si-O bond distance $\bar{r}_{\mathrm{SiO}}$ for silica glass under cold compression as obtained from ND and XRD [5,10,11], from MD simulations using either the TS (present work) or Beest-Kramer-Santen (BKS) [48,49] interatomic potentials, and from first-principles MD simulations [50]. In the present ND and MD work, $\bar{r}_{\mathrm{SiO}}$ was taken from the first peak position in $G(r)$, and $\bar{n}_{\mathrm{Si}}^{\mathrm{O}}$ was obtained by integrating over this peak to the first minimum where, if necessary, a Lorch [47] function was used to suppress Fourier transform artifacts. The ND results show an increase in $\bar{n}_{\mathrm{Si}}^{\mathrm{O}}$ above four at a pressure $> 14.5(5)$ GPa, and are consistent with the

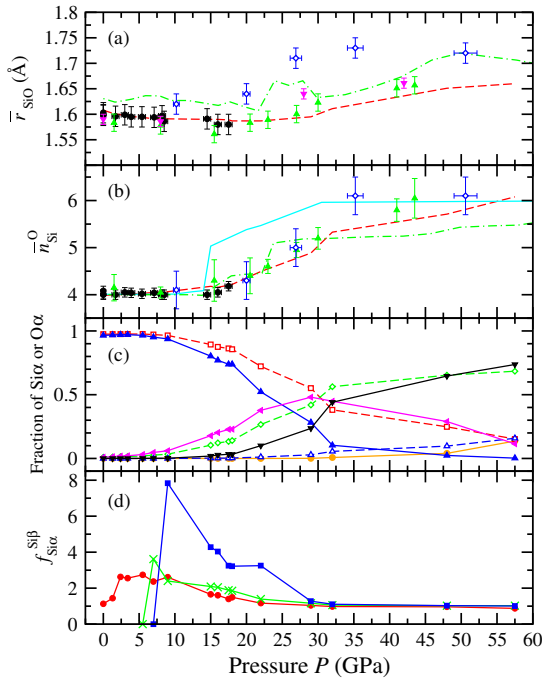

FIG. 3 (color online). The pressure dependence of the mean Si-O (a) bond distance $\bar{r}_{\mathrm{SiO}}$ and (b) coordination number $\bar{n}^{\mathrm{O}}_{\mathrm{Si}}$ as measured by ND (present work) [(black) filled circle] or by XRD in the work from Refs. [5] [(magenta) filled downward triangle], [10] [(green) filled upward triangle] and [11] [(blue) open diamond]. The results are compared to MD simulations using the TS [present work, broken (red) curves] or BKS [49] [solid (cyan) curve] potentials, and to first-principles MD simulations [50] [chained (green) curves]. (c) The pressure dependence of the fractions of Si4 [(blue) filled upward triangle], Si5 [(magenta) filled backward triangle], Si6 [(black) filled downward triangle] and Si7 [(orange) filled circle] sites and of O2 [(red) open square], O3 [(green) open diamond] and O4 [(blue) open upward triangle] sites from the TS MD simulations (present work). (d) The pressure dependence of the preference factors $f^{\mathrm{Si5}}_{\mathrm{Si5}}$ [(red) filled circle], $f^{\mathrm{Si6}}_{\mathrm{Si5}}$ [(green) ×] and $f^{\mathrm{Si6}}_{\mathrm{Si6}}$ [(blue) filled square] from the TS MD model (present work).

XRD results of Refs. [10,11] within the experimental error. The pressure dependence of $\bar{r}_{\mathrm{SiO}}$ from the work of Ref. [11] is, however, systematically different from that found from ND and from the XRD results of Refs. [5,10], which may originate from radiation induced annealing [11]. With the exception of these $\bar{r}_{\mathrm{SiO}}$ values [11], the TS model gives a good account of the measured changes in $\bar{n}^{\mathrm{O}}_{\mathrm{Si}}$ and $\bar{r}_{\mathrm{SiO}}$ over a wide pressure range extending to 60 GPa. When $\bar{n}^{\mathrm{O}}_{\mathrm{Si}}$ first increases above four, the MD simulations do not show an increase in $\bar{r}_{\mathrm{SiO}}$ but reveal an asymmetric broadening of the first peak in the Si-O partial pair-distribution function $g_{\mathrm{SiO}}(r)$ as additional oxygen atoms approach a central Si atom (Supplemental Material [30], Fig. S4). The ND results at pressures above 14.5 GPa also show this behavior as indicated by the shoulder on the high-r side of the first peak in $G(r)$ [Fig. 2(a)] and by the parameters shown in Figs. 3(a)–3(b).

The TS MD results show that, at pressures up to ~10 GPa, the network is dominated by Si4 and O2 sites [Fig. 3(c)], where the Siα and Oα notation refers to α-fold coordinated Si and O atoms, respectively. Structural changes are primarily associated with a reduction of the Si-O-Si bond angle which increases the packing fraction of SiO_4 tetrahedra. At higher pressures, the Si-O-Si bond angle reaches a minimal value of ~90° and $\bar{n}^{\mathrm{O}}_{\mathrm{Si}}$ increases via the formation of higher coordinated Si sites, where Si5 sites dominate over a window $p \sim 25$–32 GPa and Si6 sites dominate when $p \gtrsim 32$ GPa [Fig. 3(c)]. A small number of Si7 sites form when $p > 40$ GPa. To respect the glass stoichiometry, O2 sites convert to higher coordinated sites, with O3 sites becoming dominant when $p \gtrsim 30$ GPa [Fig. 3(c)].

To establish the atomistic mechanisms of network collapse under cold compression, we first consider the evolution in identity of the Si sites by finding the probability $P(\alpha, p_i \text{ and } \beta, p_j)$ that a given Si atom is α-fold coordinated at pressure p_i and β-fold coordinated at the next highest pressure p_j. As shown in Fig. 4(a), the dominant Si-O coordination number changes are $4 \rightarrow 5$ and $5 \rightarrow 6$. Few direct $4 \rightarrow 6$ changes occur (~6% at $p \sim 30$ GPa), supporting the key role played by Si5 sites as intermediaries in the transformation of silica from a low-pressure tetrahedral to a high-pressure octahedral glass.

The pressure dependence of the mean primitive ring size $\langle n \rangle \equiv \sum n\ell_n / \sum \ell_n$ is given in Fig. 4(b), where ℓ_n is the number of rings comprising a total number of n atoms. A ring is primitive if it cannot be decomposed into smaller rings [20]. The corresponding dependence of $\langle n \rangle$ on $\bar{n}^{\mathrm{O}}_{\mathrm{Si}}$ is given in the inset to Fig. 4(b). For the cold-compressed material, there is a near-linear dependence between $\langle n \rangle$ and $\bar{n}^{\mathrm{O}}_{\mathrm{Si}}$. As will be shown, this dependence can be rationalized by a densification mechanism based on successive ring-closure events, where these events result from the formation of Siα sites with $\alpha > 4$.

On cold compression, a single closure event will convert a ring of mean size $\langle n_0 \rangle$ into two rings of mean size $(\langle n_0 \rangle/2) + 1$, thereby increasing the total number of rings from N_0 to $N_0 + 1$. For m such events, it follows that $(N_0 + m)\langle n \rangle = (N_0 - m)\langle n_0 \rangle + 2m[(\langle n_0 \rangle/2) + 1] = N_0\langle n_0 \rangle + 2m$ where $\langle n \rangle$ is the mean ring size after m closures, and it is assumed that these rings remain primitive. An illustration of this process is given in the Supplemental Material [30], Fig. S6.

As shown in Fig. 4(a), the primary Si-O coordination number changes are $4 \rightarrow 5$ and $5 \rightarrow 6$. One ring closure is therefore necessary to form a Si5 site from a Si4 site, whereas two ring closures are necessary to form a Si6 site from a Si4 site. Thus, if f_α denotes the fraction of α-fold coordinated Si atoms and N_{Si} denotes the total number of Si atoms, then $m = N_{\mathrm{Si}}(f_5 + 2f_6)$. If this process were to continue *ad infinitum* then $m = N_{\mathrm{Si}} \sum_{\alpha=5}^{\infty} (\alpha - 4) f_\alpha$. Indeed, the MD results show that Si-O coordination number changes of $6 \rightarrow 7$ are common at the highest investigated

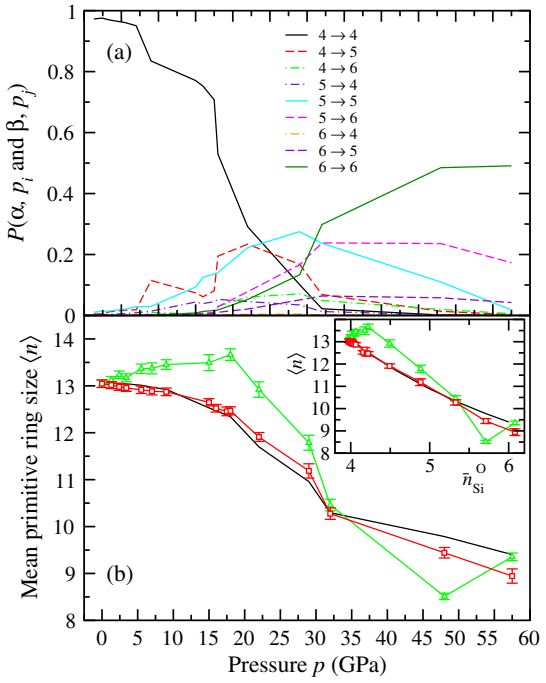

FIG. 4 (color online). (a) The pressure dependence of the probability $P(\alpha, p_i \text{ and } \beta, p_j)$ from cold-compression TS MD simulations. The $\alpha \to \beta$ labels indicate a change (broken curves) or not (solid curves) in the number α of O atoms bound to a Si atom as the pressure is increased from p_i to the next-highest value p_j. (b) The pressure dependence of the mean primitive ring size $\langle n \rangle$ from cold-compression [(red) open square] and quench-from-the-melt [(green) open triangle] TS MD simulations. The inset shows the same information but as a function of $\bar{n}_{\mathrm{Si}}^{\mathrm{O}}$. In each panel the solid (black) curve gives the prediction of the ring closure model.

pressures, but that changes of $5 \to 7$ or $4 \to 7$ are rare. Provided that no Si atom has a coordination number < 4 then $\bar{n}_{\mathrm{Si}}^{\mathrm{O}} = \sum_{\alpha=4}^{\infty} \alpha f_\alpha$ or, since $\sum_{\alpha=4}^{\infty} f_\alpha = 1$, it follows that $\bar{n}_{\mathrm{Si}}^{\mathrm{O}} = 4 + \sum_{\alpha=5}^{\infty} (\alpha - 4) f_\alpha$. Thus, $\langle n \rangle = [N_0 \langle n_0 \rangle + 2N_{\mathrm{Si}}(\bar{n}_{\mathrm{Si}}^{\mathrm{O}} - 4)]\{N_0 + N_{\mathrm{Si}}(\bar{n}_{\mathrm{Si}}^{\mathrm{O}} - 4)\}^{-1}$ or, since in the case of the TS cold-compressed MD model $N_0 = 3.98(16) N_{\mathrm{Si}} \simeq 4N_{\mathrm{Si}}$,

$$\langle n \rangle \simeq [4\langle n_0 \rangle + 2(\bar{n}_{\mathrm{Si}}^{\mathrm{O}} - 4)]/\bar{n}_{\mathrm{Si}}^{\mathrm{O}}. \quad (1)$$

As shown in Fig. 4(b), the ring closure model gives an accurate description of the cold-compression MD results for the dependence of $\langle n \rangle$ on $\bar{n}_{\mathrm{Si}}^{\mathrm{O}}$ and also for the dependence of $\langle n \rangle$ on p, where the p versus $\bar{n}_{\mathrm{Si}}^{\mathrm{O}}$ relationship was taken from MD simulations. It is notable that ~85% of the rings present at ambient pressure in the MD simulations are also present at the highest pressure, although they may no longer be primitive; i.e., many of the initial connections between Si atoms survive to high p. It is also notable that permanent densification in silica glass, which occurs at $p \gtrsim 10$ GPa [2,3,18], is associated with a change in $d\langle n \rangle/dp$ [Fig. 4(b)] but not initially with a substantial increase of $\bar{n}_{\mathrm{Si}}^{\mathrm{O}}$ above four [Fig. 3(b)]. The ring closure model does not give as accurate a description for the $\langle n \rangle$ versus $\bar{n}_{\mathrm{Si}}^{\mathrm{O}}$ or p dependence obtained from quench-from-the-melt TS MD simulations where, in accordance with the independent nature of successive liquid configurations, a negligible number ($< 1\%$) of ambient pressure rings are also present at higher p.

To highlight the spatial distribution of the evolving higher coordinated Si sites, we use the preference factor $f_{\mathrm{Si}\alpha}^{\mathrm{Si}\beta} \equiv c_{\mathrm{Si}} \bar{n}_{\mathrm{Si}\alpha}^{\mathrm{Si}\beta} / c_{\mathrm{Si}\beta} \bar{n}_{\mathrm{Si}\alpha}^{\mathrm{Si}}$ for the tendency of Siβ sites to cluster around Siα sites [51]. If there is no preference for β-fold coordinated Si atoms to occupy the Si sites that surround Siα then $f_{\mathrm{Si}\alpha}^{\mathrm{Si}\beta} = 1$. Otherwise, a preference or aversion for occupancy by β-fold coordinated Si atoms gives $f_{\mathrm{Si}\alpha}^{\mathrm{Si}\beta} > 1$ or $f_{\mathrm{Si}\alpha}^{\mathrm{Si}\beta} < 1$, respectively. The results [Fig. 3(d)] show that when Si5 or Si6 sites first emerge they are more likely to be linked to other Si5 or Si5/Si6 sites, respectively. The rings close, therefore, by a "zipper" mechanism in which a single ring closure event resulting from the formation of a higher-coordinated Siα ($\alpha > 4$) site promotes further closure events at neighboring sites, a process that helps to preserve local charge neutrality (see Supplemental Material [30], Sec. S4). An implication is that the system shows a separation into regions dominated either by Si5 and Si6 sites or by Si4 sites.

In summary, the MD results using the TS interatomic potentials give a good account of both the new ND results and the XRD results of Refs. [6,29] at pressures up to ~20 GPa. They also give a good account of the available XRD data at higher pressures in terms of the Si-O bond lengths from Refs. [5,10] and the Si-O coordination numbers from Refs. [10,11]. Fivefold coordinated Si atoms are found to act as important intermediaries in the transformation from a tetrahedral to an octahedral glass where Si6 sites dominate. A model in which rings are "zipped" by a pairing of higher-coordinated Si sites describes the simulated dependence on $\bar{n}_{\mathrm{Si}}^{\mathrm{O}}$ of the mean primitive ring size $\langle n \rangle$, which is a measure of structural ordering over multiple length scales. The role played by oxygen packing in the structural transformations that occur in SiO_2 and in other oxide glasses is described elsewhere [52].

The zipper model should be applicable to the cold compression of other chemically ordered glass-forming networks and thereby help in understanding phenomena such as permanent densification. The model also provides a coarse-grained reference for the $\langle n \rangle$ versus $\bar{n}_{\mathrm{Si}}^{\mathrm{O}}$ dependence obtained from quench-from-the-melt modeling [Fig. 4(b)], despite the reorganization of rings via diffusive processes, and will act as a guide in the development of ring closure models for modified silicate networks. All of this is important because network connectivity governs, e.g., the equation of state and transport properties for both silica and geophysically relevant silicates [12,16,53,54].

We thank Alain Bertoni, Jean-Luc Laborier, and Claude Payre for help with the D4c ND experiment (ILL), and

Keiron Pizzey, Phil Hawkins, Chris Barry, and Chris Goodway for help with the PEARL ND experiments (ISIS). The work at Bath was supported by the EPSRC via Grants No. EP/G008795/1 and No. EP/J009741/1.

*Corresponding author.
p.s.salmon@bath.ac.uk
†Corresponding author.
mark.wilson@chem.ox.ac.uk

[1] P. W. Bridgman and I. Šimon, J. Appl. Phys. **24**, 405 (1953).
[2] M. Grimsditch, Phys. Rev. Lett. **52**, 2379 (1984).
[3] R. J. Hemley, H. K. Mao, P. M. Bell, and B. O. Mysen, Phys. Rev. Lett. **57**, 747 (1986).
[4] Q. Williams and R. Jeanloz, Science **239**, 902 (1988).
[5] C. Meade, R. J. Hemley, and H. K. Mao, Phys. Rev. Lett. **69**, 1387 (1992).
[6] Y. Inamura, Y. Katayama, W. Utsumi, and K. I. Funakoshi, Phys. Rev. Lett. **93**, 015501 (2004).
[7] T. Sato and N. Funamori, Phys. Rev. Lett. **101**, 255502 (2008).
[8] V. V. Brazhkin, Phys. Rev. Lett. **102**, 209603 (2009).
[9] N. Funamori and T. Sato, Phys. Rev. Lett. **102**, 209604 (2009).
[10] C. J. Benmore, E. Soignard, S. A. Amin, M. Guthrie, S. D. Shastri, P. L. Lee, and J. L. Yarger, Phys. Rev. B **81**, 054105 (2010).
[11] T. Sato and N. Funamori, Phys. Rev. B **82**, 184102 (2010).
[12] C. Sanloup, J. W. E. Drewitt, Z. Konôpková, P. Dalladay-Simpson, D. M. Morton, N. Rai, W. van Westrenen, and W. Morgenroth, Nature (London) **503**, 104 (2013).
[13] K. Trachenko and M. T. Dove, J. Phys. Condens. Matter **14**, 7449 (2002).
[14] K. Trachenko and M. T. Dove, Phys. Rev. B **67**, 064107 (2003).
[15] K. Trachenko and M. T. Dove, Phys. Rev. B **67**, 212203 (2003).
[16] L. P. Dávila, M.-J. Caturla, A. Kubota, B. Sadigh, T. Díaz de la Rubia, J. F. Shackelford, S. H. Risbud, and S. H. Garofalini, Phys. Rev. Lett. **91**, 205501 (2003).
[17] L. Huang and J. Kieffer, Phys. Rev. B **69**, 224203 (2004).
[18] L. Huang and J. Kieffer, Phys. Rev. B **69**, 224204 (2004).
[19] L. Huang, L. Duffrène, and J. Kieffer, J. Non-Cryst. Solids **349**, 1 (2004).
[20] C. S. Marians and L. W. Hobbs, J. Non-Cryst. Solids **124**, 242 (1990).
[21] L. Stixrude and M. S. T. Bukowinski, Am. Mineral. **75**, 1159 (1990).
[22] L. Stixrude and M. S. T. Bukowinski, Phys. Rev. B **44**, 2523 (1991).
[23] Y. Liang, C. R. Miranda, and S. Scandolo, Phys. Rev. B **75**, 024205 (2007).
[24] D. A. Keen and R. L. McGreevy, Nature (London) **344**, 423 (1990).
[25] P. S. Salmon, J. W. E. Drewitt, D. A. J. Whittaker, A. Zeidler, K. Wezka, C. L. Bull, M. G. Tucker, M. C. Wilding, M. Guthrie, and D. Marrocchelli, J. Phys. Condens. Matter **24**, 415102 (2012).
[26] M. Wilding, M. Guthrie, C. L. Bull, M. G. Tucker, and P. F. McMillan, J. Phys. Condens. Matter **20**, 244122 (2008).
[27] P. Tangney and S. Scandolo, J. Chem. Phys. **117**, 8898 (2002).
[28] M. Wilson, P. A. Madden, M. Hemmati, and C. A. Angell, Phys. Rev. Lett. **77**, 4023 (1996).
[29] S. Kohara, M. Itou, K. Suzuya, Y. Inamura, Y. Sakurai, Y. Ohishi, and M. Takata, J. Phys. Condens. Matter **19**, 506101 (2007).
[30] See Supplemental Material at http://link.aps.org/supplemental/10.1103/PhysRevLett.113.135501 which contains (i) the background theory, (ii) the details of the neutron diffraction and molecular dynamics methods, (iii) some supplemental results to emphasise the validity of our approach, (iv) an illustration of a stage in the "zipper" ring closure process, and (v) Refs. [31–43].
[31] H. E. Fischer, A. C. Barnes, and P. S. Salmon, Rep. Prog. Phys. **69**, 233 (2006).
[32] V. F. Sears, Neutron News **3**, 26 (1992).
[33] P. S. Salmon, J. Phys. Condens. Matter **18**, 11443 (2006).
[34] H. E. Fischer, G. J. Cuello, P. Palleau, D. Feltin, A. C. Barnes, Y. S. Badyal, and J. M. Simonson, Appl. Phys. A **74**, s160 (2002).
[35] P. S. Salmon, Proc. R. Soc. A **445**, 351 (1994).
[36] A. Zeidler, K. Wezka, D. A. J. Whittaker, P. S. Salmon, A. Baroni, S. Klotz, H. E. Fischer, M. C. Wilding, C. L. Bull, M. G. Tucker, M. Salanne, G. Ferlat, and M. Micoulaut, Phys. Rev. B **90**, 024206 (2014).
[37] S. K. Lee, P. J. Eng, H.-K. Mao, Y. Meng, M. Newville, M. Y. Hu, and J. Shu, Nat. Mater. **4**, 851 (2005).
[38] S. Nosé, J. Chem. Phys. **81**, 511 (1984).
[39] W. G. Hoover, Phys. Rev. A **31**, 1695 (1985).
[40] G. J. Martyna, D. J. Tobias, and M. L. Klein, J. Chem. Phys. **101**, 4177 (1994).
[41] C. Meade and R. Jeanloz, Phys. Rev. B **35**, 236 (1987).
[42] O. B. Tsiok, V. V. Brazhkin, A. G. Lyapin, and L. G. Khvostantsev, Phys. Rev. Lett. **80**, 999 (1998).
[43] A. Zeidler, P. S. Salmon, R. A. Martin, T. Usuki, P. E. Mason, G. J. Cuello, S. Kohara, and H. E. Fischer, Phys. Rev. B **82**, 104208 (2010).
[44] J. W. E. Drewitt, P. S. Salmon, A. C. Barnes, S. Klotz, H. E. Fischer, and W. A. Crichton, Phys. Rev. B **81**, 014202 (2010).
[45] K. Wezka, P. S. Salmon, A. Zeidler, D. A. J. Whittaker, J. W. E. Drewitt, S. Klotz, H. E. Fischer, and D. Marrocchelli, J. Phys.: Condens. Matter **24**, 502101 (2012).
[46] E. Soignard, C. J. Benmore, and J. L. Yarger, Rev. Sci. Instrum. **81**, 035110 (2010).
[47] E. Lorch, J. Phys. C **2**, 229 (1969).
[48] B. W. H. van Beest, G. J. Kramer, and R. A. van Santen, Phys. Rev. Lett. **64**, 1955 (1990).
[49] J. S. Tse, D. D. Klug, and Y. Le Page, Phys. Rev. B **46**, 5933 (1992).
[50] M. Wu, Y. Liang, J.-Z. Jiang, and J. S. Tse, Sci. Rep. **2**, 398 (2012).
[51] L. B. Skinner, A. C. Barnes, P. S. Salmon, L. Hennet, H. E. Fischer, C. J. Benmore, S. Kohara, J. K. R. Weber, A. Bytchkov, M. C. Wilding, J. B. Parise, T. O. Farmer, I. Pozdnyakova, S. K. Tumber, and K. Ohara, Phys. Rev. B **87**, 024201 (2013).
[52] A. Zeidler, P. S. Salmon, and L. B. Skinner, Proc. Natl. Acad. Sci. U.S.A. **111**, 10045 (2014).
[53] C. A. Angell, P. A. Cheeseman, and S. Tamaddon, Science **218**, 885 (1982).
[54] S. K. Lee, G. D. Cody, Y. Fei, and B. O. Mysen, Geochim. Cosmochim. Acta **68**, 4189 (2004).

High-Pressure Transformation of SiO_2 Glass from a Tetrahedral to an Octahedral Network: A Joint Approach Using Neutron Diffraction and Molecular Dynamics

Supplemental Material

Anita Zeidler,[1] Kamil Wezka,[1] Ruth F. Rowlands,[1] Dean A. J. Whittaker,[1]
Philip S. Salmon,[1,*] Annalisa Polidori,[1] James W. E. Drewitt,[2]
Stefan Klotz,[3] Henry E. Fischer,[4] Martin C. Wilding,[5]
Craig L. Bull,[6] Matthew G. Tucker,[6] and Mark Wilson[7,†]

[1] *Department of Physics, University of Bath, Bath, BA2 7AY, United Kingdom*
[2] *Centre for Science at Extreme Conditions, School of Physics and Astronomy, University of Edinburgh, Edinburgh EH9 3JZ, United Kingdom*
[3] *IMPMC, CNRS UMR 7590, Université Pierre et Marie Curie, 75252 Paris, France*
[4] *Institut Laue Langevin, 6 rue Jules Horowitz, BP 156, 38042 Grenoble, France*
[5] *IMPS, Aberystwyth University, Aberystwyth SY23 3BZ, United Kingdom*
[6] *ISIS Facility, Rutherford Appleton Laboratory, Chilton, Didcot, Oxon OX11 0QX, United Kingdom*
[7] *Physical and Theoretical Chemistry Laboratory, University of Oxford, South Parks Road, Oxford OX1 3QZ, United Kingdom*

[*] Corresponding author: p.s.salmon@bath.ac.uk
[†] Corresponding author: mark.wilson@chem.ox.ac.uk

S1. BACKGROUND THEORY

In a neutron or x-ray diffraction experiment on silica (i.e. SiO_2) glass the total structure factor

$$S(k) = 1 + \sum_{\alpha} \sum_{\beta} \frac{c_\alpha c_\beta f_\alpha(k) f^*_\beta(k)}{|\langle f(k) \rangle|^2} [S_{\alpha\beta}(k) - 1] \tag{S1}$$

is measured, where α and β denote the chemical species, c_α represents the atomic fraction of chemical species α, $f_\alpha(k)$ and $f^*_\alpha(k)$ are the form factor (or scattering length) for chemical species α and its complex conjugate, respectively, k is the magnitude of the scattering vector, $\langle f(k) \rangle = \sum_\alpha c_\alpha f_\alpha(k)$ is the mean form factor (or scattering length), and $S_{\alpha\beta}(k)$ is a partial structure factor [1]. In the case of neutron diffraction, the scattering lengths are independent of k and are given by $f_{\mathrm{Si}} = 4.1491(10)$ fm and $f_{\mathrm{O}} = 5.803(4)$ fm [2].

In practice, a diffractometer can only access a finite k-space range with a maximum cutoff value $k_{\max}$ such that $S(k)$ is truncated by a modification function $M(k)$ where $M(k) = 1$ for $k \leq k_{\max}$, $M(k) = 0$ for $k > k_{\max}$. The real-space information corresponding to $S(k)$ is obtained from the Fourier transform relation

$$G(r) = 1 + \frac{1}{2\pi^2 \rho r} \int_0^\infty \mathrm{d}k\, k\, [S(k) - 1]\, M(k) \sin(kr) \tag{S2}$$

where $G(r)$ is the total pair-distribution function and ρ is the atomic number density. This equation leads to a convolution of the desired r-space information with the Fourier transform of $M(k)$. The severity of the Fourier transform artifacts in $G(r)$ that are associated with using a step function for $M(k)$ can be reduced by using instead a Lorch [3] function, albeit at the expense of a broadening of r-space features. The Lorch function is given by $M(k) \equiv \sin(ak)/(ak)$ for $k \leq k_{\max}$, $a = \pi/k_{\max}$, and $M(k) = 0$ for $k > k_{\max}$ where a rigorous derivation is given in Ref. [4]. To facilitate a like-for-like comparison between measured and molecular dynamics results, the reciprocal-space functions constructed from simulations can be Fourier transformed according to Eq. (S2) using the $M(k)$ function that was applied to the experimental data.

S2. METHODS

A. Neutron Diffraction

Two sets of *in situ* high-pressure neutron diffraction experiments were performed at a temperature T ∼300 K on solid pellets of silica glass (GE 214, impurity content < 25 ppm), shaped to fit the anvils of a Paris-Edinburgh press. The first set employed the diffractometer D4c [5] at ambient pressure, 1.7(5), 3.0(5), 3.9(5), 5.4(5), 7.1(5) and 8.2(5) GPa, and used the experimental and data analysis procedures described in Refs. [6, 7] but with an incident wavelength of 0.4951(1) Å to enhance the measured k-range. The second set employed the time-of-flight diffractometer PEARL at pressures (p) of 8.5(5), 14.5(5), 16.0(5) and 17.5(5) GPa, and used the experimental and data analysis protocols described in Ref. [8]. In this second set of experiments, the region $k \leq 1.55$ Å^{-1} was not accessible and an extrapolation of $S(k)$ to smaller k-values was made by fitting a Lorenztian function to the measured first sharp diffraction peak (FSDP), which has a peak position of $k_{\rm FSDP} = 1.82(2)$ Å^{-1} at $p = 8.5$ GPa versus $k_{\rm FSDP} = 2.23(2)$ Å^{-1} at $p = 17.5$ GPa. The FSDP for glassy materials often has a Lorentzian profile [9], and this was confirmed by the fits that were obtained to the measured $S(k)$ functions. In the low-k region there is also agreement within the statistical error between the fitted Lorentzian function for the PEARL data at $p = 8.5$ GPa and the measured D4c $S(k)$ data set at $p = 8.2$ GPa for which the minimum k-value is 0.3 Å^{-1} (Fig. 1(a)). The measured Si-O bond distances and coordination numbers were not found to be sensitive to the details of the Lorentzian fitting procedure.

In a high-pressure neutron diffraction experiment, the sample is held within the anvils of a press by a Ti-Zr gasket, and scattering from this gasket can make a significant contribution to measured diffraction patterns [6, 8]. The robustness of the PEARL results was investigated by repeating the data analysis using the diffraction patterns for both unsquashed and squashed (i.e. recovered from $p = 17.5$ GPa) Ti-Zr gaskets as measured during the same experimental run or during different experimental runs. For a given pressure point, the observed deviations in the Si-O bond distance $\bar{r}_{\rm SiO}$ and coordination number $\bar{n}^{\rm O}_{\rm Si}$ were within the error bars plotted in Figs. 3(a) and 3(b). In a separate set of high-pressure experiments on glassy GeO_2, the robustness of PEARL $S(k)$ and $G(r)$ functions was tested extensively, and the results were found to be in agreement with those obtained from independent neutron

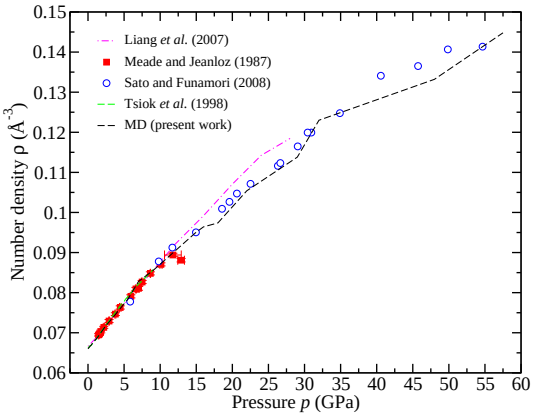

Fig. S1. The pressure-density equation of state for SiO_2 glass under cold compression where p denotes the pressure and ρ denotes the atomic number density. The measured data sets from Meade and Jeanloz [12] [(red) ■ with error bars], Tsiok *et al.* [13] [broken light (green) curve], and Sato and Funamori [14] [(blue) ○] are compared to the results obtained from molecular dynamics simulations using the TS interatomic potentials [15] in the present work [broken (black) curve] and in the work by Liang *et al.* [19] [chained (magenta) curve].

diffraction experiments that used the diffractomter D4c with a markedly different experimental setup [8]. In a neutron diffraction investigation of B_2O_3 glass at pressures up to 17.5 GPa [10], the B-O coordination numbers measured using PEARL were found to be in agreement within the experimental error with those obtained from inelastic x-ray scattering experiments [11].

The pressure-dependent number densities used in the data analysis were taken from Refs. [12–14] and are shown in Fig. S1.

B. Molecular Dynamics

The molecular dynamics simulations with the Tangney-Scandolo (TS) potentials [15] used reduced charges of $2.76514e$ and $-1.38257e$ for the Si and O ions, respectively, where e denotes the elementary charge. An equilibrated liquid at 4000 K was first generated within the NVT ensemble using $N = 999$ ions and a volume V chosen to give the density of the ambient pressure glass. The corresponding glass was prepared by selecting 100 independent liquid configurations separated by ∼100 ps, significantly longer than the relaxation time probed by the intermediate scattering function. Each configuration was quenched to 300 K

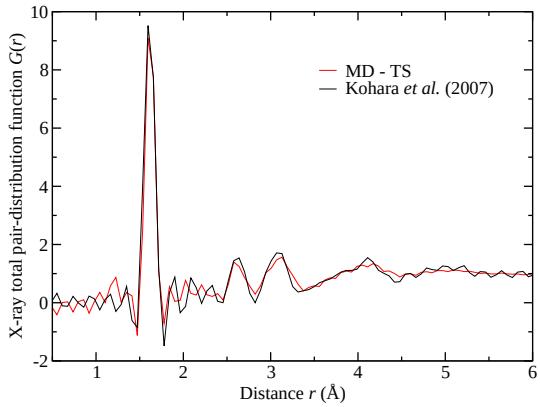

Fig. S2. The x-ray total pair-distribution function $G(r)$ for SiO_2 glass at ambient pressure as obtained by Fourier transforming the measured x-ray total structure factor of Kohara *et al.* [20] shown in Fig. 1(b) [solid (black) curve]. The solid light (red) curve gives the result obtained by Fourier transforming the molecular dynamics x-ray total structure factor shown in Fig. 1(b) after truncating at the same cut-off $k_{\max} = 35$ Å^{-1} as used for the measured data set. The sole or main contributors to the first three peaks in $G(r)$ are the Si–O, O–O and Si–Si partial pair-distribution functions, respectively.

at a rate of $\sim 10^{15}$ K s^{-1} using a Nosé-Hoover thermostat [16, 17] and run on for ∼100 ps.

High-pressure glasses were prepared by cold-compressing each of the 100 glass configurations obtained from the previous (lower) pressure using the NpT ensemble with a barostat [18]. The resultant configurations were then equilibrated within the NVT ensemble for ∼100 ps. High-pressure glasses were also prepared by using a quench-from-the-melt protocol in which a liquid state configuration taken from the previous (lower) pressure was compressed within the NpT ensemble before equilibrating within the NVT ensemble. One hundred independent configurations were then selected for quenching to the glass and equilibrating as above. The investigated pressures were ambient, 1.3, 2.4, 3.4, 5.5, 7, 9, 15, 16, 17.5, 18, 22, 29, 32, 48 and 57.5 GPa.

In Fig. S1, the measured equation of state for SiO_2 glass under cold compression is compared to the results obtained from molecular dynamics simulations using the TS interatomic potentials in the present work and in the work of Liang *et al.* [19].

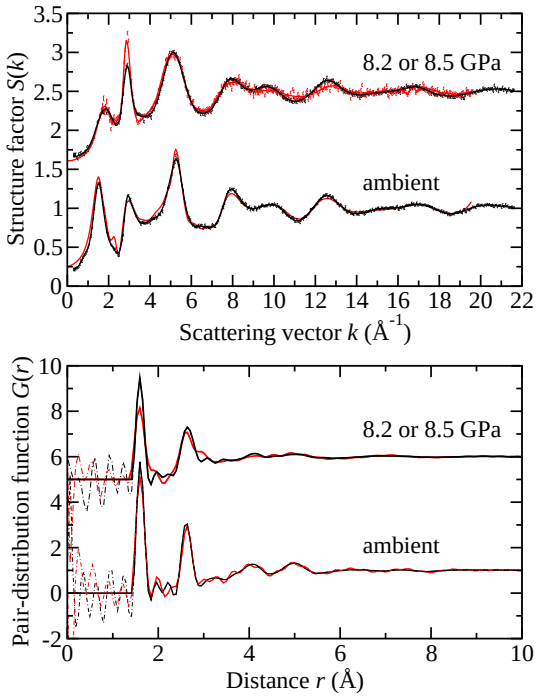

Fig. S3. A comparison of (a) the total structure factor $S(k)$ and (b) the total pair-distribution function $G(r)$ as measured for SiO_2 glass in a Paris-Edinburgh press using the diffractometers D4c [dark (black) symbols and curves] and PEARL [light (red) symbols and curves] at ambient pressure and at a pressure of 8.2(5) GPa (D4c) or 8.5(5) GPa (PEARL). In (a) the vertical bars give the statistical errors on the measured data points, and the solid curves give spline fits. In the case of the PEARL experiments, the region $k \leq 1.55$ Å^{-1} was not accessible and the solid curves for this region correspond to fitted Lorentzian functions [8]. In (b) the solid curves show the Fourier transforms of the solid curves given in (a), and the broken curves show the associated Fourier transform artifacts at r-values smaller than the distance of closest approach between two atoms.

S3. SUPPLEMENTAL RESULTS

At ambient pressure, the molecular dynamics simulations using the TS interatomic potentials [15] give a good account of the measured x-ray total pair-distribution function $G(r)$ [20] (Fig. S2).

Fig. S3(a) compares the $S(k)$ functions for SiO_2 glass as measured using the diffractometers D4c and PEARL at ambient pressure and at a pressure of 8.2(5) or 8.5(5) GPa. Each of the data sets was measured with the sample held in a Paris-Edinburgh press but with different scattering geometries [6, 8]. At ambient pressure, the error bars on the PEARL

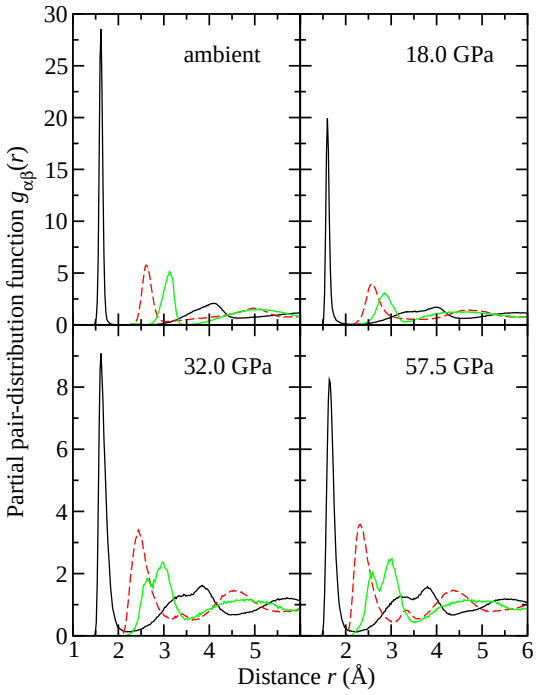

Fig. S4. The Si-O [dark solid (black) curves], O-O [broken (red) curves] and Si-Si [light solid (green) curves] partial pair-distribution functions from cold-compression molecular dynamics simulations using the TS interatomic potentials at several pressures.

$S(k)$ function are comparatively large and are omitted for clarity of presentation. The corresponding $G(r)$ functions are shown in Fig. S3(b). At ambient conditions, the D4c and PEARL $G(r)$ functions are in excellent agreement. There is, however, a broadening of the features in the PEARL $G(r)$ function at 8.5(5) GPa compared to the D4c $G(r)$ function at 8.2(5) GPa. This broadening is consistent with the higher pressure of the PEARL measurement, although its magnitude is surprising given the similarity in pressure values. Some of the discrepancy shown in Fig. 2(a) between the PEARL and molecular dynamics $G(r)$ functions may therefore arise from experimental artifacts. In high-pressure experiments on glassy B_2O_3, a broadening of the first peak in $G(r)$ is also found for a PEARL data set measured at 8.5 GPa compared to a D4c data set measured at 8.2 GPa [10]. In high-pressure experiments on glassy $GeSe_4$ and As_2Se_3, however, no broadening of the first peak in $G(r)$ is observed for PEARL data sets measured at 8.5 GPa compared to D4c data sets measured at 8.2 GPa (K. J. Pizzey, private communication).

Fig. S4 compares the partial pair-distribution functions $g_{\alpha\beta}(r)$ from the cold-compression TS molecular dynamics results for several different pressures. The first peak in $g_{\mathrm{SiO}}(r)$ shows

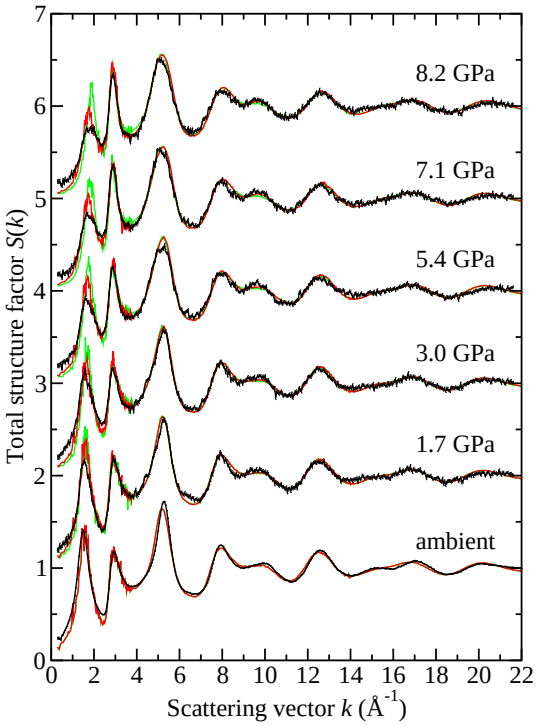

Fig. S5. The neutron total structure factor $S(k)$ for SiO_2 glass at different pressures as measured using the diffractometer D4c [solid (black) curve with vertical error bars] and as calculated from molecular dynamics using the TS interatomic potentials [15] with either a cold-compression [solid light (red) curves] or quench-from-the-melt [solid light (green) curves] protocol.

an asymmetric broadening with increasing pressure as it develops a high-r tail.

Fig. S5 compares several of the measured neutron total structure factors $S(k)$ with those obtained from molecular dynamics simulations using the TS interatomic potentials [15] with either a cold-compression or quench-from-the-melt protocol. The cold-compression results give a better representation of the measured data sets, especially in the region of the first-sharp diffraction peak at $k_{\rm FSDP}$ $\sim$1.5–1.8 Å^{-1}. Some of the remaining discrepancy in the region of this peak between the neutron diffraction and cold-compression molecular dynamics results can be attributed to the asymmetric k-space resolution function of the neutron diffractometer D4c used for the experiments [21].

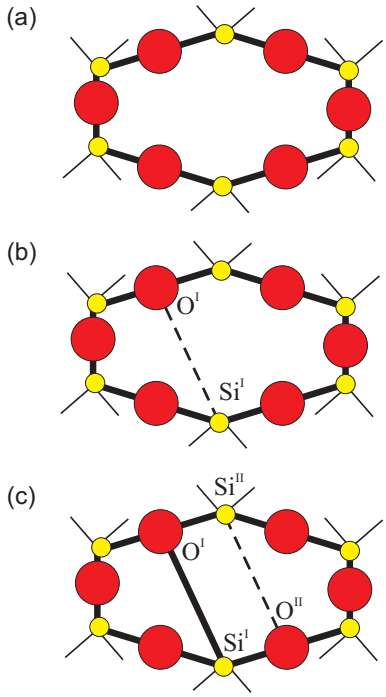

Fig. S6. Schematic of a ring comprising a total of 12 atoms (a) before a closure event, (b) after a single closure event, and (c) after two closure events. Within a ring, the small (yellow) circles represent Si atoms and the large (red) circles represent O atoms. At a given stage in the densification process, existing Si-O bonds within a ring are shown by solid thick lines and the new Si-O bond is shown by a broken line. The remainder of the Si-O bonds are indicated by solid thin lines.

S4. STAGE IN THE "ZIPPER" RING CLOSURE PROCESS

To illustrate a stage in the densification procedure based on successive ring-closure events, consider a system with mean ring size $\langle n_0 \rangle$ where a schematic for one of the rings is shown in Fig. S6(a). Let a silicon atom labeled Si^I close the ring by forming a bond with the oxygen atom labeled O^I thus making the Si^I atom fivefold coordinated and the O^I atom threefold coordinated (Fig. S6(b)). The ring closure event creates two new rings of mean size $\langle n' \rangle = (\langle n_0 \rangle /2) + 1$. Now let a second silicon atom labeled Si^{II} close one of the new rings by forming an edge-sharing connection with Si^I such that Si^{II} also becomes fivefold coordinated and O^{II} becomes threefold coordinated (Fig. S6(c)). This ring closure event creates two new rings of mean size $\langle n'' \rangle = (\langle n' \rangle /2) + 1$. Hence, after two ring closure events,

the overall mean ring size is given by

$$\begin{aligned}\langle n\rangle &= \frac{1}{3}\left[\langle n'\rangle + 2\langle n''\rangle\right] \\ &= \frac{2}{3}\left[\langle n'\rangle + 1\right] \\ &= \frac{1}{3}\left[\langle n_0\rangle + 4\right] \end{aligned} \tag{S3}$$

which also follows from the equation $(N_0+m)\langle n\rangle = N_0\langle n_0\rangle+2m$ given in the main text since the initial number of rings $N_0 = 1$ and the number of ring-closure events $m = 2$. Fig. S6(c) illustrates a case in which a ring is "zipped" by the formation of a pair of higher-coordinated Siα ($\alpha > 4$) sites.

In the above, let the initial ring in Fig. S6(a) be formed from corner-sharing SiO_4 tetrahedra in a chemically ordered network. Then each Si atom is bound to 4 twofold coordinated O atoms such that the Si:O ratio is 1:2, in keeping with the glass stoichiometry. After the first ring closure event, the Si^{I} atom is bound to 4 twofold coordinated O atoms and 1 threefold coordinated oxygen atom such that the Si^{I}:O ratio is 1:(4/2 + 1/3) or 1:2.33. After the second ring closure event, the Si^{I} and Si^{II} atoms are each bound to 3 twofold coordinated O atoms and 2 threefold coordinated oxygen atoms such that the $Si^{I/II}$:O ratio is 1:(3/2 + 2/3) or 1:2.17. The zipping of the initial ring by a pairing of higher-coordinated Siα atoms therefore acts in a direction to help preserve locally the glass stoichiometry. Since the Si and O atoms in the TS interatomic potentials are charged, this preservation of stoichiometry promotes charge neutrality at a local level.

---

[1] H. E. Fischer, A. C. Barnes, and P. S. Salmon, Rep. Prog. Phys. **69**, 233 (2006).

[2] V. F. Sears, Neutron News **3**, 26 (1992).

[3] E. Lorch, J. Phys. C: Solid State Phys. **2**, 229 (1969).

[4] P. S. Salmon, J. Phys.: Condens. Matter **18**, 11443 (2006).

[5] H. E. Fischer, G. J. Cuello, P. Palleau, D. Feltin, A. C. Barnes, Y. S. Badyal, and J. M. Simonson, Appl. Phys. A **74**, S160 (2002).

[6] J. W. E. Drewitt, P. S. Salmon, A. C. Barnes, S. Klotz, H. E. Fischer, and W. A. Crichton, Phys. Rev. B **81**, 014202 (2010).

[7] K. Wezka, P. S. Salmon, A. Zeidler, D. A. J. Whittaker, J. W. E. Drewitt, S. Klotz, H. E. Fischer, and D. Marrocchelli, J. Phys.: Condens. Matter **24**, 502101 (2012).

[8] P. S. Salmon, J. W. E. Drewitt, D. A. J. Whittaker, A. Zeidler, K. Wezka, C. L. Bull, M. G. Tucker, M. C. Wilding, M. Guthrie, and D. Marrocchelli, J. Phys.: Condens. Matter **24**, 415102 (2012).

[9] P. S. Salmon, Proc. R. Soc. Lond. A **445**, 351 (1994).

[10] A. Zeidler, K. Wezka, D. A. J. Whittaker, P. S. Salmon, A. Baroni, S. Klotz, H. E. Fischer, M. C. Wilding, C. L. Bull, M. G. Tucker, M. Salanne, G. Ferlat, and M. Micoulaut, Phys. Rev. B **90**, 024206 (2014).

[11] S. K. Lee, P. J. Eng, H.-K. Mao, Y. Meng, M. Newville, M. Y. Hu, and J. Shu, Nature Mater. **4**, 851 (2005).

[12] C. Meade and R. Jeanloz, Phys. Rev. B **35**, 236 (1987).

[13] O. B. Tsiok, V. V. Brazhkin, A. G. Lyapin, and L. G. Khvostantsev, Phys. Rev. Lett. **80**, 999 (1998).

[14] T. Sato and N. Funamori, Phys. Rev. Lett. **101**, 255502 (2008).

[15] P. Tangney and S. Scandolo, J. Chem. Phys. **117**, 8898 (2002).

[16] S. Nosé, J. Chem. Phys. **81**, 511 (1984).

[17] W. G. Hoover, Phys. Rev. A **31**, 1695 (1985).

[18] G. J. Martyna, D. J. Tobias, and M. L. Klein, J. Chem. Phys. **101**, 4177 (1994).

[19] Y. Liang, C. R. Miranda, and S. Scandolo, Phys. Rev. B **75**, 024205 (2007).

[20] S. Kohara, M. Itou, K. Suzuya, Y. Inamura, Y. Sakurai, Y. Ohishi, and M. Takata, J. Phys.: Condens. Matter **19**, 506101 (2007).

[21] A. Zeidler, P. S. Salmon, R. A. Martin, T. Usuki, P. E. Mason, G. J. Cuello, S. Kohara, and H. E. Fischer, Phys. Rev. B **82**, 104208 (2010).